Title
High-speed fiber based polarization-sensitive optical coherence tomography of in vivo human skin.

Journal
Optics letters, 25(18)

ISSN
0146-9592

Authors
Saxer, CE
de Boer, JF
Park, BH
et al.

Publication Date
2000-09-01

DOI
10.1364/ol.25.001355

High-speed fiber–based polarization-sensitive optical coherence tomography of *in vivo* human skin

Christopher E. Saxer, Johannes F. de Boer, B. Hyle Park, Yonghua Zhao, Zhongping Chen, and J. Stuart Nelson

Beckman Laser Institute and Medical Clinic, University of California, Irvine, Irvine, California 92612

Received March 16, 2000

A high-speed single-mode fiber–based polarization-sensitive optical coherence tomography (PS OCT) system was developed. With a polarization modulator, Stokes parameters of reflected flight for four input polarization states are measured as a function of depth. A phase modulator in the reference arm of a Michelson interferometer permits independent control of the axial scan rate and carrier frequency. *In vivo* PS OCT images of human skin are presented, showing subsurface structures that are not discernible in conventional OCT images. A phase retardation image in tissue is calculated based on the reflected Stokes parameters of the four input polarization states. © 2000 Optical Society of America

OCIS codes: 170.0170, 170.4500, 260.1440, 260.5430, 110.7050, 170.1870.

Optical coherence tomography (OCT) is an emerging technology for noninvasive imaging of biological tissue. Based on a Michelson interferometer, the technique measures spatially resolved reflected intensity in tissue, offering a dynamic range in excess of 100 dB.[1] The development of polarization-sensitive optical coherence tomography (PS OCT) has permitted additional information on the polarization properties of tissue carried by the reflected light to be obtained.[2–6] Many biological tissues such as tendon, muscle, nerve, bone, cartilage, and teeth exhibit birefringence because of their linear or fibrous structure.[7] The advantages of PS OCT are enhanced contrast and specificity in identifying structures in OCT images by detection of changes induced in the polarization state of light that reflected from the sample.

Previous PS OCT systems were air-spaced interferometers that used bulk optical components that permitted precise control over the polarization state of light in the sample and reference arms.[2–6] Fiber-based interferometers offer distinct advantages in terms of system alignment and handling but pose design problems owing to polarization changes induced in optical fibers. Polarization-maintaining (PM) fibers have large birefringence with a beat length of 2–3 mm. The energy of wave components along the primary axes of the fiber is preserved, but the relative phase is lost owing to the difference in experienced optical path length. To determine the Stokes parameters, such phase information is needed.[5]

Single-mode (SM) fibers have polarization-mode dispersion (PMD). Because of the random birefringence induced by core ellipticity and noncircularly symmetric stresses, SM fibers propagate two nearly degenerate orthogonal polarization states. Differential phase delay (DPD) and differential group delay between these two states cause, respectively, an evolution of the polarization states along the fiber and a broadening of the interferogram in an OCT system. For fiber length L shorter than mode-coupling length h, DPD and differential group delay are directly proportional to fiber length. This relationship changes into a square-root dependence for $L \gg h$, indicating the underlying one-dimensional random-walk nature of PMD.[8] We used a single-mode fiber (Corning SMF-28) with a PMD $\leq 0.1\ \mathrm{ps}/\sqrt{\mathrm{km}}$ if $L > h$ and $\leq 0.1\sqrt{\mathrm{km}}/\sqrt{h}\ \mathrm{ps/km}$ if $L < h$, which yields an optical path-length difference between orthogonal polarization states that is in either case less than 2 μm for 4.4 m of fiber.

In Fig. 1 a single-mode fiber–based PS OCT system is presented. We minimized the total PMD by using a short fiber length in the sample arm (1.75 m) and in the reference arm (45 cm SM; 75 cm PM). A low-coherence source (AFC Technologies) with a FWHM bandwidth of 80 nm centered at 1310 nm was polarized by a bulk polarizer and coupled back into the fiber. Quarter- and half-wave plates before the polarizer were used to select the polarization state of the source with the highest power (8 mW). Quarter- and half-wave plates after the polarizer prepared the polarization such that after a short fiber length (15 cm) the light emerged with equal-magnitude wave components parallel and perpendicular to the optic axis of a bulk electro-optic polarization modulator (New Focus 4104). The modulator permits control of the polarization state over a grand circle on Poincaré's sphere, as shown in Fig. 2. The dashed grand circle indicates the possible polarization states immediately

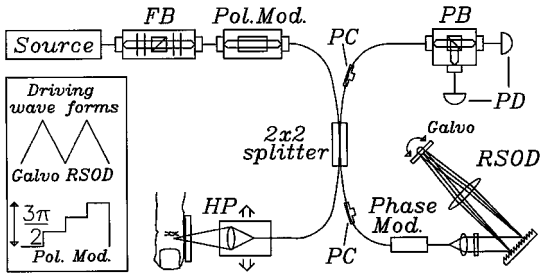

Fig. 1. Schematic of the fiber-based PS OCT system. Source: 1310 nm, 80-nm bandwidth; FB, fiber bench with bulk polarizer and quarter- and half-wave plates; Pol. Mod., $LiNbO_3$ polarization modulator mounted in fiber bench; PC's, static polarization controllers; PB, polarizing beam splitter; PD, photo diodes; Phase Mod., phase modulator; RSOD, defined in text; HP, hand piece mounted upon a motorized linear translation stage. Driving waveforms to the galvo of the RSOD and the polarization modulator show their respective timings.

0146-9592/00/181355-03$15.00/0

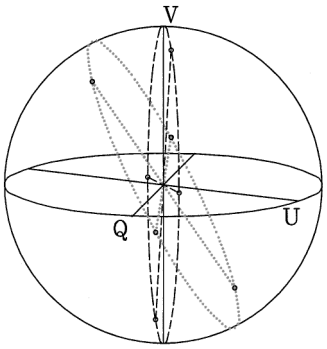

Fig. 2. Poincaré's sphere, with the Q, U, and V axes indicated. The dashed grand circle and axes show the possible polarization states after the polarization modulator. The dotted grand circle and axes show a realization of the polarization states at the sample arm fiber tip as a result of PMD. The angles between the Stokes vectors are maintained in the absence of polarization-dependent loss.

after the modulator. A four-step driving function, in which each step introduces a $\pi/2$ phase shift, cycles the light over four Stokes vectors, indicated by the dashed axes in the grand circle, before a fiber 2×2 coupler. In the reference arm, a static polarization controller is aligned such that for all four polarization states half of the light is transmitted through a PM fiber pigtailed phase modulator (JDS Uniphase), which by its structure polarizes the light. The PM fiber is also used to couple the light into a rapid-scanning optical delay line (RSOD),[9,10] which is operated with the spectrum centered on the galvo mirror. The RSOD thus generates only a group delay and no phase delay; the carrier of the interferometric signal at the detector is generated only by the phase modulator. The phase modulator is driven by a sawtooth waveform at 1 MHz, generating a maximum 2π phase shift after double passage. The sample arm consists of a fiber with a collimator and a focusing lens mounted upon a motorized linear translation stage. As a result of DPD, the polarization state at the tip of the sample arm fiber is unknown. However, in a lossless fiber (with a total differential group delay smaller than the coherence time of the light), the transformations in Poincaré's sphere are orthonormal, preserving the angles between the four Stokes vectors. The dotted grand circle and axes in Fig. 2 indicate a possible realization of the four polarization states at the fiber tip. In the detection arm a static polarization controller before the polarizing beam splitter is aligned such that the light from the reference arm is split equally over both detectors. Electronic signals are high-pass filtered, amplified, and digitized by a 12-bit dual-channel 10-Msamples/s per channel analog–digital board (Gage Applied Sciences Inc.).

Data processing consists of lock-in detection in software of the sine and cosine components at the reference frequency of 1 MHz. The sine and cosine components of 5-μm segments in each A line (depth profile) of 2-mm length are processed to yield the Stokes parameters as described earlier[5,7]:

$$I = \sin_H{}^2 + \cos_H{}^2 + \sin_V{}^2 + \cos_V{}^2 , \quad (1)$$

$$Q = \sin_H{}^2 + \cos_H{}^2 - \sin_V{}^2 - \cos_V{}^2 , \quad (2)$$

$$U = 2 \sin_H \times \sin_V + 2 \cos_H \times \cos_V , \quad (3)$$

$$V = 2 \sin_H \times \cos_V - 2 \cos_H \times \sin_V , \quad (4)$$

where $\sin_{H,V}$ and $\cos_{H,V}$ are the sine and cosine components; subscripts H and V indicate, respectively, the horizontal and vertical polarization channels; and I, Q, U, and V are the Stokes parameters.

Figure 3 shows a set of four images (I, Q, U, and V) of human skin from the finger of a volunteer subject for a single-input polarization state. The finger was pressed against a glass slide with index-matching fluid to reduce the surface reflection from the tissue. Obvious changes are visible in Stokes images Q, U, and V, which indicate the presence of structures that are not seen in reflectivity image I that are changing the polarization state of the light.

Figure 4 shows the results of using a polarization modulator to image human skin from the forearm of a volunteer subject. Modulating the incident light over four polarization states generates 16 images, 4 for each input state. The RSOD was driven by a 624-Hz triangular waveform, and the polarization modulator was driven by a 312-Hz four-step waveform. The velocity of the linear translation stage was 1.56 mm/s, and the scan took 2 s. Figure 4 shows a set of two images (A and B) containing the information from these 16 images.

We constructed the first image (A) by averaging the reflectivity images of the four different input states. The second image was constructed as follows: The four different input states lay along perpendicular axes on a grand circle in Poincaré's sphere; two pairs of input states were collinear but in opposite directions. Their Stokes parameters Q, U, and V differed by only a minus. The Stokes parameter images Q, U, and V for such an input pair were very similar, except for the minus. For each pair we averaged the I images by addition and the Q, U, and V images by subtraction. The resulting eight images (one set of I, Q, U, and V images per input pair) define two Stokes vectors that are described by lengths I_1 and I_2 and three component (Q, U, and V) vectors $\mathbf{S}_1$ and $\mathbf{S}_2$ with unit length.

The second image (B) is a phase-retardation map of the tissue, constructed form the two vectors $\mathbf{S}_1$ and $\mathbf{S}_2$. First, the average states $\overline{\mathbf{S}}_1$ and $\overline{\mathbf{S}}_2$ reflected from the glass–tissue interface were calculated, which defined our input states. Next, a single rotation matrix $\mathbf{R}$ was calculated that simultaneously transformed $\overline{\mathbf{S}}_1$

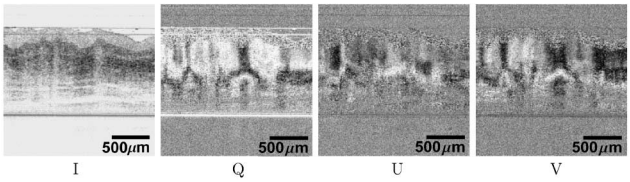

Fig. 3. PS OCT images of *in vivo* human finger skin; 2 mm $\times$ 2 mm, pixel size 5 μm $\times$ 5 μm. Left to right, Stokes parameters I, Q, U, and V for a single input polarization state. The images are gray-scale coded over a 40-dB range for I and from 1 to -1 for Q, U, and V.

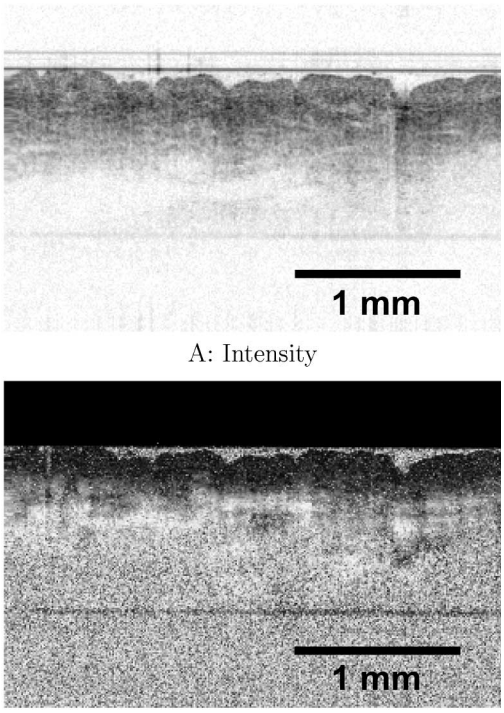

Fig. 4. PS OCT images of *in vivo* human forearm skin, 2 mm × 3.1 mm, pixel size 5 μm × 5 μm for A, the intensity image and 10 μm × 10 μm for B, the phase-retardation image. The images are gray-scale coded over 40 dB for intensity and from 0 (black) to π (white) for the phase retardation. For a description of the data processing, see the text.

to $\mathbf{S}_1$ and $\overline{\mathbf{S}}_2$ to $\mathbf{S}_2$ at each position in the image. An exact solution will not always exist. We determined the best solution for $\mathbf{R}$ by calculating the angles ϕ_1 between $(\mathbf{R} \cdot \overline{\mathbf{S}}_1)$ and $\mathbf{S}_1$ and ϕ_2 between $(\mathbf{R} \cdot \overline{\mathbf{S}}_2)$ and $\mathbf{S}_2$ and minimizing the sum of the angles, weighted by the absolute length of the Stokes vector, $(\phi_1 I_1 + \phi_2 I_2)|_{\min}$. The phase retardation, gray-scale coded from 0 to π, is given by the rotation angle of matrix $\mathbf{R}$. Although the exact polarization states with which the sample is probed are unknown, an image showing phase retardation can be constructed from the measurements with four different input states. The phase-retardation image reveals birefringent structures at a depth of 300 μm below the surface, which we attribute to the presence of collagen in the dermis of human skin.

Currently, a single-rotation matrix is calculated at each depth in the sample; this assumes that the optical axis is constant. In a more advanced approach, the rotation matrix could be calculated between consecutive Stokes vectors along a depth profile, which would take into account variations in the orientation of the optic axis with depth. The total encountered birefringence would be the sum of the absolute values of the consecutive rotation angles. However, the presence of speckle noise would likely lead to a significant overestimation of the total phase retardation.

In conclusion, we have demonstrated a fiber-based PS OCT system that is capable of measuring birefringence of *in vivo* human skin. We achieved insensitivity to DPD in the sample arm fiber and orientation of the optic axis in tissue by modulating across four different input polarization states. Noninvasive measurement of collagen birefringence could be an important parameter in the assessment of burn depth, as collagen is denatured as a result of thermal damage, leading to a reduction in birefringence.[11]

Research grants from the Whitaker Foundation (grant 26083 to J. F. de Boer), the National Eye Institute (1 R24 EY 12877-01), the U.S. Office of Naval Research (N00014-94-1-0874), the Institute of Arthritis, Musculoskeletal and Skin Diseases, the U.S. Department of Energy, and the Beckman Laser Institute Endowment are gratefully acknowledged. J. F. de Boer's e-mail address is deboer@bli.uci.edu.

References

1. D. Huang, E. A. Swanson, C. P. Lin, J. S. Schuman, W. G. Stinson, W. Chang, M. R. Hee, T. Flotte, K. Gregory, C. A. Puliafito, and J. G. Fujimoto, Science **254,** 1178 (1991).
2. M. R. Hee, D. Huang, E. A. Swanson, and J. G. Fujimoto, J. Opt. Soc. Am. B **9,** 903 (1992).
3. J. F. de Boer, T. E. Milner, M. J. C. van Gemert, and J. S. Nelson, Opt. Lett. **22,** 934 (1997).
4. M. J. Everett, K. Schoenenberger, B. W. Colston, Jr., and L. B. Da Silva, Opt. Lett. **23,** 228 (1998).
5. J. F. de Boer, T. E. Milner, and J. S. Nelson, Opt. Lett. **24,** 300 (1999).
6. G. Yao and L. V. Wang, Opt. Lett. **24,** 537 (1999).
7. J. F. de Boer, S. M. Srinivas, B. H. Park, T. H. Pham, Z. Chen, T. E. Milner, and J. S. Nelson, IEEE J. Sel. Top. Quantum Electron. **5,** 1200 (1999).
8. C. D. Poole, Opt. Lett. **13,** 687 (1988).
9. G. J. Tearney, B. E. Bouma, and J. G. Fujimoto, Opt. Lett. **22,** 1811 (1997).
10. A. M. Rollins, M. D. Kulkarni, S. Yazdanfar, R. Ung-arunyawee, and J. A. Izatt, Opt. Express **3,** 219 (1998), http://epubs.osa.org/opticsexpress.
11. J. F. de Boer, S. S. Srinivas, A. Malekafzali, Z. Chen, and J. S. Nelson, Opt. Express **3,** 212 (1998), http://epubs.osa.org/opticsexpress.